

PAPER

Hydrogen sensing via anomalous optical absorption of palladium-based metamaterials

To cite this article: A Hierro-Rodriguez *et al* 2016 *Nanotechnology* **27** 185501

View the [article online](#) for updates and enhancements.

Related content

- [On the anodic aluminium oxide refractive index of nanoporous templates](#)
A Hierro-Rodriguez, P Rocha-Rodrigues, F Valdés-Bango *et al*.
- [Engineering metallic nanostructures for plasmonics and nanophotonics](#)
Nathan C Lindquist, Prashant Nagpal, Kevin M McPeak *et al*.
- [Diamond like carbon nanocomposites with embedded metallic nanoparticles](#)
Sigita Tamulevius, Šarnas Meškinis, Tomas Tamulevius *et al*.

Hydrogen sensing via anomalous optical absorption of palladium-based metamaterials

A Hierro-Rodriguez^{1,2}, I T Leite^{2,4}, P Rocha-Rodrigues¹, P Fernandes^{1,2},
J P Araujo^{1,3}, P A S Jorge², J L Santos^{2,3}, J M Teixeira^{1,5} and A Guerreiro^{2,3}

¹ IFIMUP and IN—Institute of Nanoscience and Nanotechnology, Rua Campo Alegre, 4169-007 Porto, Portugal

² INESC-TEC (Coordinated by INESC-Porto), Rua Campo Alegre, 4169-007 Porto, Portugal

³ Departamento de Física e Astronomia, Faculdade de Ciências, Universidade do Porto, Rua Campo Alegre, 4169-007 Porto, Portugal

E-mail: ahierro@fc.up.pt

Received 24 September 2015, revised 8 December 2015


Accepted for publication 29 February 2016

Published 22 March 2016



Abstract

A palladium (Pd)-based optical metamaterial has been designed, fabricated and characterized for its application in hydrogen sensing. The metamaterial can replace Pd thin films in optical transmission schemes for sensing with performances far superior to those of conventional sensors. This artificial material consists of a palladium–alumina metamaterial fabricated using inexpensive and industrial-friendly bottom-up techniques. During the exposure to hydrogen, the system exhibits anomalous optical absorption when compared to the well-known response of Pd thin films, this phenomenon being the key factor for the sensor sensitivity. The exposure to hydrogen produces a large variation in the light transmission through the metamembrane (more than 30% with 4% in volume hydrogen–nitrogen gas mixture at room temperature and atmospheric pressure), thus avoiding the need for sophisticated optical detection systems. An optical homogenization model is proposed to explain the metamaterial response. These results contribute to the development of reliable and low-cost hydrogen sensors with potential applications in the hydrogen economy and industrial processes to name a few, and also open the door to optically study the hydrogen diffusion processes in Pd nanostructures.

 Online supplementary data available from stacks.iop.org/NANO/27/185501/mmedia

Keywords: hydrogen sensing, optical metamaterial, nanoporous aluminum oxide templates

(Some figures may appear in colour only in the online journal)

1. Introduction

Hydrogen is one of the most promising chemical elements for use in fuel cells and combustion engines that produce a clean energy. Therefore, it is extensively used in scientific research and industry, refining petroleum products, and in the chemical industry in general [1–3]. However, it is a colorless and

odorless gas, highly explosive in the presence of oxygen with a lower ignition concentration limit of 4% in ambient atmospheric conditions. These properties are a drawback in the exploitation of H₂-based technologies that could be circumvented by the development of high-sensitivity, inexpensive and reliable sensors to detect H₂. Conventional H₂ sensors are often large, in general expensive, operate mostly at high temperatures (100 °C–300 °C) and suffer from poor selectivity towards H₂. They are based on metal-oxide chemiresistors, thermal conductors, catalytic and electrochemical processes [4, 5]. In contrast, forefront H₂ sensors operate at

⁴ Present address: School of Engineering, Physics, and Mathematics, University of Dundee, Dundee DD1 4HN, UK.

⁵ Present address: Depto. de Física, Facultad de Ciencias, Universidad de Oviedo, C/Calvo Sotelo s/n, 33007 Oviedo, Spain.

room temperature, are less bulky and more sensitive to H_2 . They are based on nanostructures and/or thin films of certain metals, mostly palladium (Pd) and Pd alloys, which experience a reversible change in their electrical, optical and structural properties upon exposure to H_2 [5–12]. In fact, Pd undergoes a reversible phase transition from metal to metal hydride (Pd_α and Pd_β phases), when hydrogen is inserted within the Pd crystal lattice [13]. Among this variety of H_2 sensors, the optical detection is considered a very promising approach due to its inherent safe nature when compared to the electric counterparts (elimination of electric currents in H_2 atmospheres minimizes the risk of explosion and is therefore highly desirable for all H_2 -related applications), high sensitivity in ambient atmospheric conditions, short response times and low power consumption.

There have been a number of attempts to utilize plasmonic effects to increase the sensitivity of hydrogen sensors. The first demonstration is reported in [14] using surface plasmon polaritons at the Pd/air interface in the Kretschmann configuration. The problem is that all these Pd-based plasmonic sensors suffer from poor sensitivity, owing to the very broad optical spectral resonance profiles of Pd, and lack of reliability. To overcome this limitation, hybrid plasmonic systems of Au/Pd have been designed and fabricated in several configurations, ranging from long-range plasmon polaritons observed in thin films [15], nanowires (NWs) [16], optical fibers [17] and gratings [18], to localized surface plasmons presented in nanoparticles and disks [19–21]. Despite these attempts, the sensitivity enhancement remains limited and/or requires expensive fabrication techniques and/or sophisticated optical configurations.

In this work, a Pd-based optical metamaterial is presented from fundamental design to final implementation and experimental testing. It consists of a nanoporous anodized aluminum oxide (AAO) template which hosts Pd NWs. The material behaves as a variable light absorber and can be used as a highly sensitive optical H_2 sensor. It works in transmission of non-polarized light at normal incidence through the metamaterial slab. The metamaterial's light absorption increases when it is exposed to H_2 . This is unexpected and contradicts the Pd thin film's behavior, where the transition from pure metal to Pd_α and Pd_β phases increases the dielectric character of the metal, leading to a reduction in light absorption [22, 23]. To our knowledge, this anomalous optical absorption is reported here for the first time in Pd-based metamaterials. Simple optical homogenization models take account of the metamaterial's behavior, allowing not only to predict the sensor response, but also opening the door to study the H diffusion processes inside Pd nanostructures. The sensor response time, sensitivity, repeatability and feasibility are competitive with or even greater than those of other optical state-of-the-art approaches based on Pd [7, 8], including some which are based on plasmonic enhanced effects [16, 17] without using expensive fabrication and/or characterization schemes.

The article is organized as follows: first of all the theoretical design of the metamaterial is presented by using both Bruggeman's and Maxwell–Garnett optical

homogenization. It is used to analyze the performance of the future sensor and to identify the better metamaterial's parameters. This section is followed by the explanation of fabrication and optical characterization techniques. After that, the experimental results are discussed starting with a description of the anomalous optical absorption and an explanation of its origin. The system's behavior is discussed in terms of both H_2 sensing capabilities and H diffusion processes inside the Pd NWs. Finally, the main remarks of the manuscript are presented in the Conclusion section.

2. Metamaterial design

The proposed metamaterial sensor is based on amorphous AAO templates where the nanopores are filled with Pd NWs, forming an optical metamaterial membrane (or metamembrane). The optical properties of the metamembrane are determined by the metallic NW and AAO refractive indices and also by the template's structural parameters. During H_2 exposure, the Pd NWs undergo a phase transition from pure metallic Pd to Pd hydride, changing their refractive index. The Pd hydride presents two different phases with different optical properties depending on the Pd–H atomic concentration. Pure Pd_α is formed for very low H atomic concentrations (below 2%) while pure Pd_β appears only above a concentration of 58% [13]. In between, a mixture of both phases defines the optical properties of the Pd hydride. In this framework, the calculation of the optical properties of the Pd hydride, which forms the NWs, is performed using Bruggeman's homogenization model [24, 26]. The refractive index of the metamaterial as a whole is done by applying the Maxwell–Garnett theory [25, 26]. We are allowed to use these homogenization approaches because the different Pd_α and Pd_β domains inside the NWs and the characteristic template structural parameters, namely the AAO lattice parameter (a) and pore diameter (d_p), are typically smaller than the optical wavelengths ($a \approx 100$ nm and $d_p \approx 35$ nm).

$$\sum_{i=1}^N f_i \frac{\varepsilon_i - \varepsilon_{\text{eff}}}{\varepsilon_i + \eta \varepsilon_{\text{eff}}} = 0, \quad (1)$$

$$\varepsilon_{\text{eff}} = \varepsilon_h \frac{1 + \eta \Gamma}{1 - \Gamma}, \quad \Gamma = \sum_{i=1}^N f_i \frac{\varepsilon_i - \varepsilon_h}{\varepsilon_i + \eta \varepsilon_h}, \quad (2)$$

Equations (1) and (2) show the effective electric permittivity (ε_{eff}) expressions for the Bruggeman and Maxwell–Garnett models respectively for an arbitrary number N of material inclusions. In both sets of equations f_i and ε_i represent respectively the fill ratio and the electric permittivity of the i th inclusion, ε_h is the electric permittivity of the host medium (in this case the AAO template) and η is the screening factor of the inclusions. The latter depends on the inclusion's shape regarding electric field orientation and is defined as $\eta = L^{-1} - 1$, where L is the Lorentz depolarization factor. The Pd_β/Pd_α mixture inside the NWs is assumed to be homogeneous due to the very short diffusion time of H in the NWs [27] and due to this, it is better described by the

Bruggeman model. The different Pd hydride phase domains are considered spherical, leading to a $\eta = 2$, and the fill ratio in this first homogenization is identical to the $\text{Pd}_\beta/\text{Pd}_\alpha$ ratio. On the other hand, the metamaterial as a whole consists of an AAO template where the pores are filled with Pd NWs comprising well-separated optical domains. Therefore, it is better described by the Maxwell–Garnett model with $\eta = 1$, corresponding to high aspect ratio cylinders oriented parallel to the incident light wave vector. The fill ratio of the NWs inside the AAO template is defined as $f_{\text{AAO}} = (4\pi^2/3)^{1/2} \cdot (d_p/2a)^2$ and relates the structural parameters with a geometric factor. The effective dielectric constants and corresponding refractive indices obtained from these effective medium models depend on the electric permittivity of Pd_α , Pd_β and AAO. At this point, we have assumed that the electric permittivity of the metallic Pd and Pd_α phase are almost the same due to the low H atomic concentration needed for the formation of the Pd_α hydride. Hence, the data for metallic Pd and Pd_β are obtained from [22] and [23], respectively, and the refractive index for the AAO is taken from spectroscopic ellipsometry measurements of an aluminum oxide amorphous thin film sputter deposited on a Si substrate (see more details about the refractive indices in the supplementary material).

A scheme of the metamaterial is presented in figure 1(a). It shows the hexagonal arrangement of the Pd NWs inside the AAO template and indicates the main structural parameters, a , d_p and membrane thickness (l). In figure 1(b), the complex refractive index of a metamembrane with $a = 92$ nm and $d_p = 43$ nm ($f_{\text{AAO}} \approx 20\%$) has been calculated as a function of free-space wavelength by performing the homogenization process previously mentioned. Real (n , left-side scale) and imaginary (κ , right-side scale) parts are shown for Pd_α (continuous black line) and Pd_β (dashed red line) NWs inside the AAO template. The behavior of the imaginary part of the refractive index for Pd_α and Pd_β metamembranes exhibits a clear peak for wavelengths around 290 nm due to the localized surface plasmon resonance present at the interface between the NWs and the AAO membrane. There is no shift in the peak position between both states of the Pd NWs. Nevertheless, a strong reduction of the peak's amplitude (20%) and also a broadening are observed after changing from Pd_α to Pd_β NWs. The first effect can be understood by the decrease of NWs' metallic nature after the hydrogenation, as can be seen from the decrease in the imaginary part of the Pd hydride refractive index when compared with the value of pure Pd [22, 23, 28, 29]. The second effect (peak broadening) is responsible for a phenomenon in the visible spectral range. In this range, the extinction coefficient for the Pd_β metamembrane is larger (33% on average) than for the Pd_α . It constitutes a form of anomalous light absorption because, as mentioned before, the κ value of a Pd thin film decreases when exposed to H_2 . Finite difference time-domain (FDTD) electrodynamic simulations have been performed using the MEEP code [30] to verify that this effect is not an artifact from the homogenization models. Both the homogenization models (figure 1(c)) and the FDTD simulations (figure 1(d)) qualitatively agree, showing a decrease in light transmittance

corresponding to the anomalous absorption. Therefore, this effect in the Pd metamaterial is predicted and well described by the homogenization models, allowing to use them to compute the light transmission through the metamembrane.

A change in the Pd_α to Pd_β ratio due to the exposure of H_2 alters the complex refractive index and the total amount of light transmitted through the metamembrane. Part of the light is absorbed as it propagates within the metamaterial. In particular, the fraction of light absorbed (A) and transmitted in the bulk (T^{bulk}) depends only on the thickness l and the imaginary part of the refractive index κ of the metamembrane and can be written as follows as a function of wavelength (λ).

$$A = 1 - T^{\text{bulk}}, \quad T^{\text{bulk}} = \exp\left(\frac{-2\pi}{\lambda}(\kappa \cdot l)\right), \quad (3)$$

Another part of the light is reflected as it crosses the interface between the metamembrane and the surrounding gas. The amount of light transmitted (T^{inter}) and reflected (R^{inter}) at the interface between the two media at normal incidence depends mainly on the real part of the refractive index n since it is much larger than κ (figure 1(b)) and it can be calculated using the Fresnel equations [31] leading to equation (4).

$$T^{\text{inter}} = 1 - R^{\text{inter}}, \quad R^{\text{inter}} \approx \frac{(n_g - n_m)^2}{(n_g + n_m)^2}, \quad (4)$$

The labels g and m refer respectively to the gas and the metamaterial. The overall transmittance of the metamembrane as a function of the Pd_α to Pd_β ratio (represented by x , $x = 0$ for pure Pd_α and $x = 1$ for pure Pd_β) is:

$$T(x) = T^{\text{inter}}(x) \cdot T^{\text{bulk}}(x) \cdot T^{\text{inter}}(x). \quad (5)$$

Due to the small variation in n_m while changing from Pd_α to Pd_β in the visible range, $R^{\text{inter}}(x) \approx R^{\text{inter}}(0)$, then $T^{\text{inter}}(x) \approx T^{\text{inter}}(0)$. Taking this into account, the relative transmittance variation, which is defined as $\delta T(x)$, can be approximated as follows.

$$\delta T(x) \approx \frac{T^{\text{bulk}}(x) - T^{\text{bulk}}(0)}{T^{\text{bulk}}(0)}. \quad (6)$$

This implies that $\delta T(x)$ is mainly dependent on the κ_m variation during the Pd hydrogenation, meaning that the absorption effects are mainly responsible for the H_2 metamaterial sensitivity. Therefore, $\delta T(x)$ works as a figure of merit for the sensitivity of the sensor. In this framework, we have engineered the metamaterial structure to analyze the performance of the final sensor.

In figure 2, the reflectance variation (ΔR) of the air/metamembrane interface after considering pure Pd_α or Pd_β NWs (figure 2(a)), the transmittance T through a 1- μm -thick metamembrane embedded in air (figure 2(b)) and the relative variation in transmittance δT of the metamembrane (figure 2(c)) are shown as a function of the AAO fill ratio and

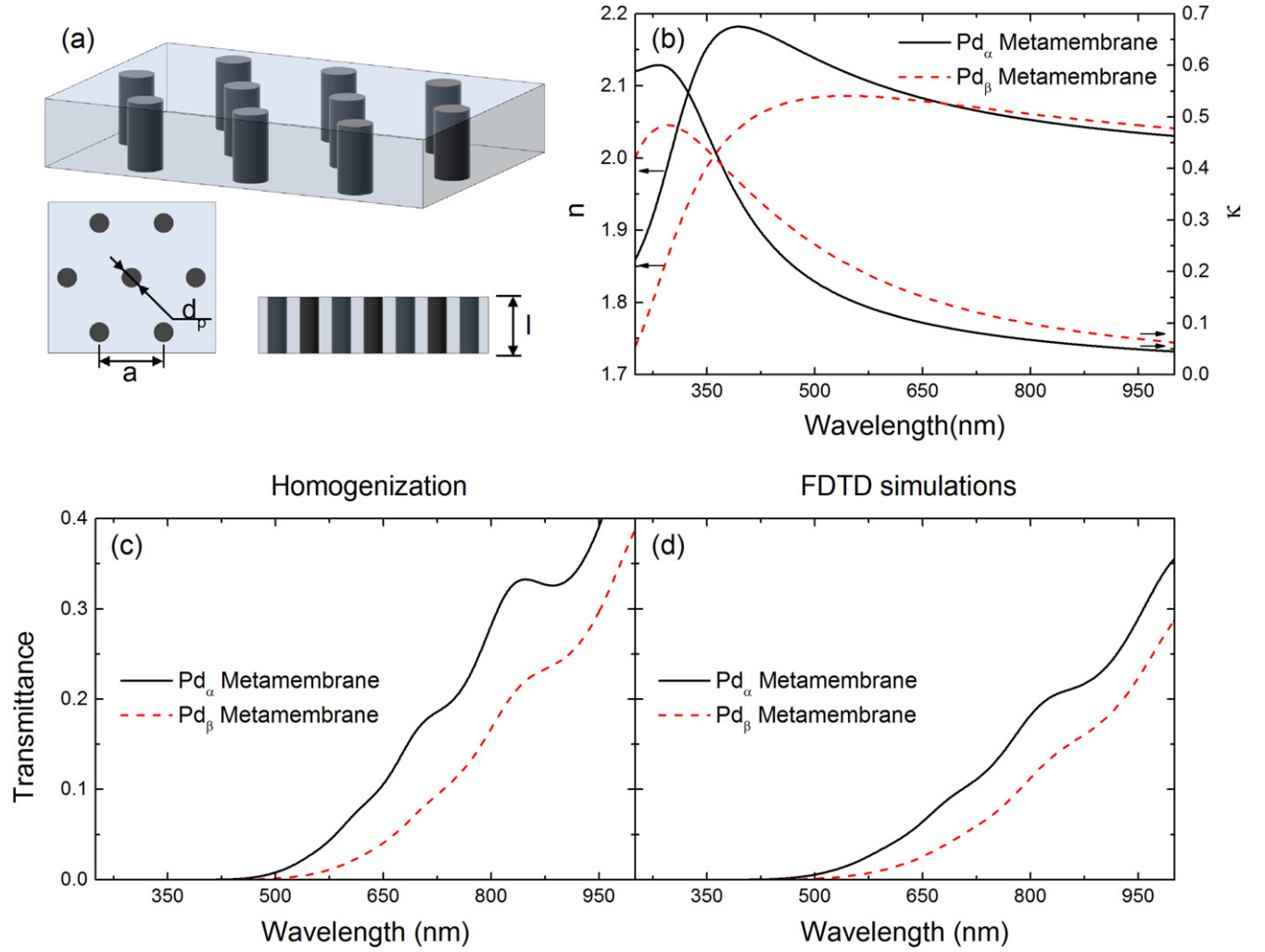


Figure 1. (a) Scheme of an AAO template filled with Pd NWs, showing the main structural parameters: lattice parameter (a), NW diameter (d_p) and metamembrane thickness (l). (b) Real (left scale) and imaginary (right scale) parts of complex refractive indices for Pd_α (continuous black line) and Pd_β (dashed red line) metamembranes as a function of wavelength, computed by homogenization models. Transmittances as a function of wavelength obtained by (c) Maxwell-Garnett homogenization model and (d) finite difference time-domain simulations for Pd_α (continuous black line) and Pd_β (dashed red line) metamembranes.

Pd_β phase concentration for a constant wavelength of 633 nm. Figure 2(a) shows the negligible variation in reflectance upon considering all possible Pd_α to Pd_β ratios and also all possible AAO fill ratios [$\Delta R = R_{g/m}(x, f_{AAO}) - R_{g/m}(0, f_{AAO})$]. Three possible designs for the metamaterial are identified by the dashed vertical lines A, B and C in all the panels. A fill ratio of about 10% (line A) corresponds to the highest transmittance and offers the best signal-to-noise ratio but also leads to low δT , implying that the sensor would have poor sensitivity. On the other hand, for fill ratios of about 60% (line B), the metamaterial presents the best sensitivity (at least for low H concentrations) but only a small fraction of light would be transmitted through the metamembrane (low transmittance region in figure 2(b)), requiring the use of intense optical sources. Fill ratios of about 20% (line C) balance sensor sensitivity and show a reasonable optical throughput, with transmittances between 3% and 9% and a decrease in δT up to 50% for pure Pd_β NWs. Based on these considerations, a metamembrane sample with the later AAO

fill ratio ($f_{AAO} \approx 20\%$) has been fabricated to be characterized and tested as an optical H_2 gas sensor.

3. Metamaterial fabrication and optical characterization setup

The AAO template was fabricated by a standard two-step anodization process in 0.3 M oxalic acid ($H_2C_2O_4$) from high-purity (99.997%) Al foils [32–34]. A first 24 h anodization at 40 V was performed to obtain a good order in the resulting nanopore lattice. After this, the obtained AAO membrane was removed by selective wet etching, and the Al film was again anodized under the same conditions for 8 h. This leads to a membrane with a thickness of about 20 μm which keeps the previously obtained lattice order. Then, a pore widening process (wet etching) to increase the natural fill ratio of the template to $\sim 20\%$ was performed and, finally, the Pd NW growth was done using the pulsed electrodeposition method

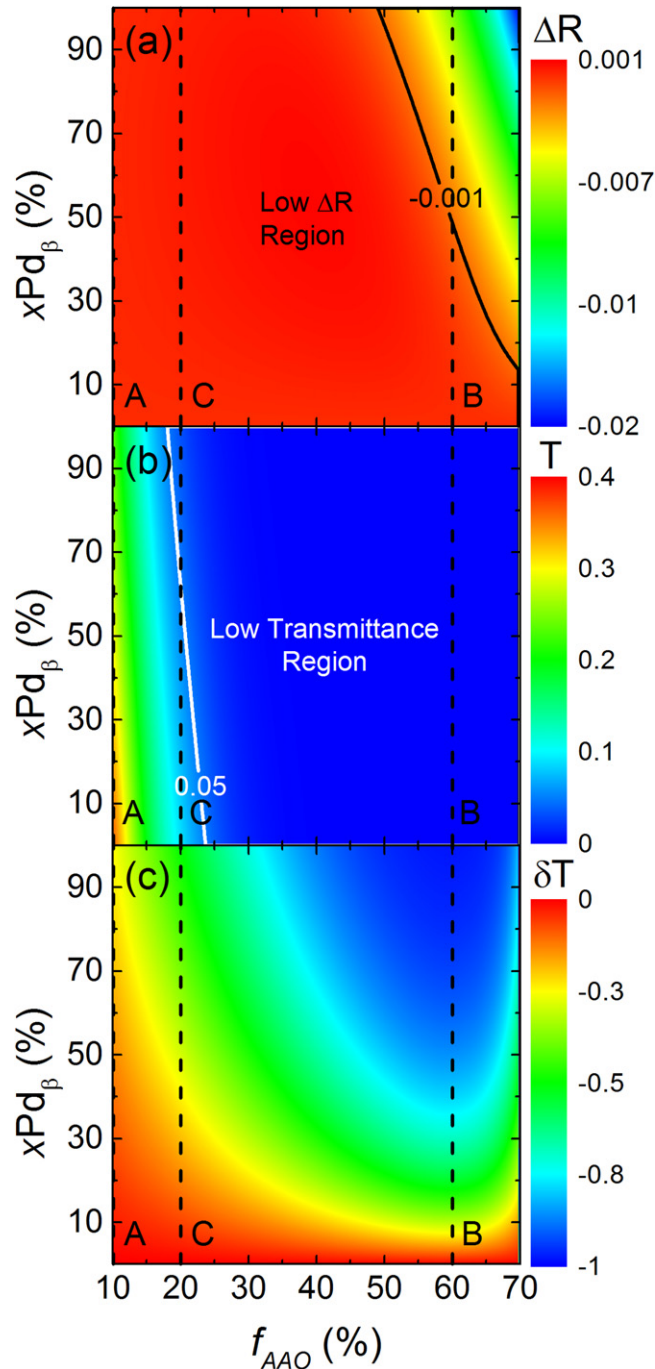


Figure 2. (a) Reflectivity change at the Air/Pd metamaterial interface for $\lambda = 633$ nm as a function of AAO fill ratio and Pd_β phase concentration inside the NWs. (b) Transmittance (T) and (c) relative transmittance change (δT) predicted by the model for the metamaterial at $\lambda = 633$ nm as a function of AAO fill ratio and Pd_β phase concentration. Vertical dashed lines at 10% (A), 60% (B) and 20% (C) of AAO fill ratio indicate the best T , the best δT and the good operation region selected for the optical sensor, respectively.

[35] in a Pd salt-based solution after dendrite formation. A more detailed description of the used reagents, concentrations and processes is available in the provided supplementary material.

Representative images of the sample taken in a cross-section and a top view using scanning electron microscopy

(SEM) are shown in figures 3(a) and (b), respectively. Bright and dark gray contrasts relate to the Pd NWs and the AAO template, respectively. The SEM images were used to determine the average structural parameters of the fabricated metamaterial ($a \sim 90$ nm, $d_p \sim 45$ nm) which correspond to a fill ratio of 23%. The cross-section image shows dispersion in the NW lengths corresponding to an average $l_{\text{NW}} \sim 1.3$ μm inside a 23- μm -thick AAO membrane. To allow for transmission light measurements through the metamembrane, a circular hole on the back side of the Al foil was made by selective chemical etching (figure 3(a) inset) and the dendrites were removed from that area by Ar^+ ion beam etching.

The experimental setup for the optical characterization and testing of the metamaterial sensor is shown in figure 3(c). It consists of a gas chamber with multiple feedthroughs: for gas injection, for the vacuum system and for optical fibers. The gas sources were two high-purity mixtures of H_2 in N_2 (4% and 1% in volume, nominal) and pure N_2 .

Different partial pressures of H_2 can be achieved by changing the total pressure of the gas mixture inside the chamber, so, for low H_2 pressures, the 1% concentration source at low total pressure was used, and for high partial pressures, the 4% concentration bottle at high pressure was selected (typical max. total pressure ~ 6 atm). A fiberoptic tungsten-halogen light source was connected to the illumination collimator (blue fiber), then the collimated light passed through the metamembrane and was collected by another optical fiber collimator. The outgoing fiber (red fiber) was connected to an optical fiber charge coupled device spectrometer allowing us to record the sample's optical response.

4. Results and discussion

4.1. Anomalous optical absorption

The explanation for the anomalous absorption observed was investigated using FDTD simulations of a single Pd NW (in α and β phases) embedded in a dielectric medium with a refractive index of 1.6 (similar to the measured value for the Al_2O_3 sputter-deposited thin film). Different parameters were extracted from the simulations: the scattering (figure 4(a)) and absorption (figure 4(b)) cross-sections, and also the electric field in the central longitudinal slice of the computational space (centered with the NW). The former were studied using a broad frequency source, thus obtaining the spectral response of these parameters, and the latter was recorded at a fixed frequency source ($\omega \approx 2.9 \times 10^{15}$ rad s^{-1} , equivalent to $\lambda_0 = 650$ nm) for the analysis of the electric field configuration. From figures 4(a) and (b) we demonstrate that the scattering of light in the NW is not responsible for the anomalous absorption because it is almost independent on the $\text{Pd}_\alpha/\text{Pd}_\beta$ phases. Even at smaller wavelengths (< 500 nm), the Pd_α NW scatters more than the Pd_β NW, as expected by their refractive index differences.

Instead, the origin of the anomalous light absorption phenomenon comes from the way in which optical power is distributed between the NW and the surrounding AAO

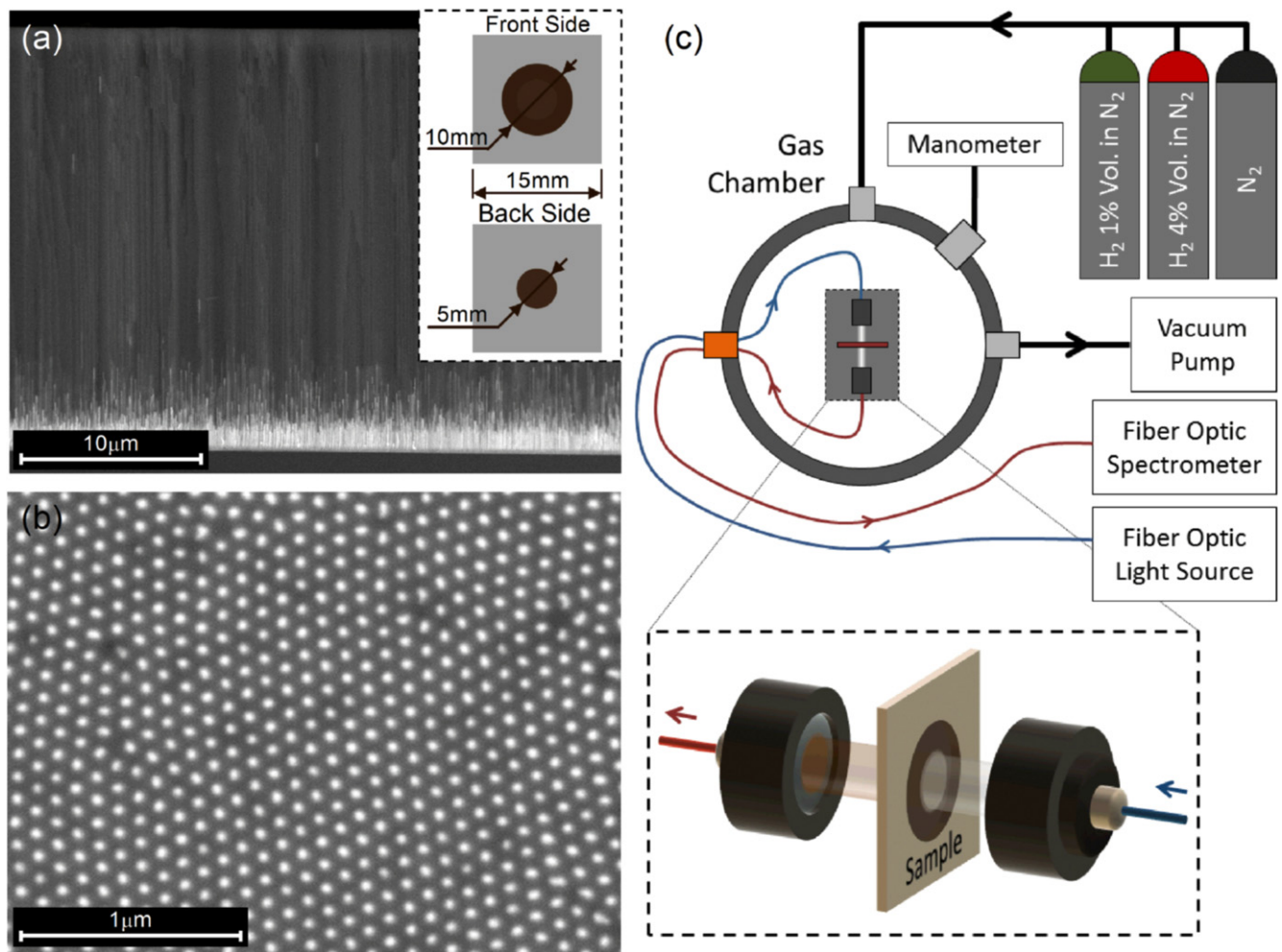


Figure 3. (a) SEM cross-section micrograph before removing the dendrites and (b) top view micrograph after dendrite removal of the sample's back side. A sample's scheme is shown in inset. (c) Experimental setup layout for the transmission measurements inside the gas chamber; blue and red fibers indicate light injection and collection systems, respectively.

matrix. During the hydrogenation process, the imaginary part of the Pd refractive index decreases, leading to a decrease in the optical absorption. This suggests that the metamaterial would become more transparent. However, one observes an increase in absorption, in agreement with the imaginary part of the Pd_β metamembrane effective refractive index shown in figure 1(b). As the light enters the metamaterial along the direction of the wire, part of the optical power of the incident beam propagates through the Pd NW while other goes through the AAO dielectric matrix. The ratio between these two power fractions strongly depends on the refractive index of the wires and ultimately on the state of hydrogenation of the Pd. Hence, when the Pd_α transforms into Pd_β , both the imaginary part of the refractive index of the NW and the optical impedance between the NW and the AAO matrix decrease. This allows more optical power to be transferred from the AAO matrix into the NW, where it is strongly absorbed. The fact can be observed in figures 4(c) and (d) where the $|E_x|^2$ is presented for a longitudinal slice centered in the simulation box, and it is also noted in figure 4(e), which shows a field profile along the center of the NW. The first and second images refer to Pd_α and Pd_β NWs, respectively, and

the color scale is the same for both. It is clearly shown that in the Pd_β case a more intense electric field is present inside the NW than in the Pd_α state, illustrating the previous hypothesis.

4.2. Metamaterial sensor characterization

The metamaterial light transmission spectra as a function of time were recorded for different partial H_2 pressures inside the gas chamber. This allows one to study the behavior of light transmission as a function of H_2 partial pressure. For each different pressure, we defined H_2 charge and discharge times. During the former, the gas inside the chamber was injected from one of the two H_2 gas mixtures, and for the discharge time, only pure N_2 is present inside the chamber, allowing the H to be released from the Pd metamembrane. There is no gas flow during the measurements, and the total pressure in both sequences was kept constant. This charge/discharge sequence was repeated under the same pressure conditions several times, forming different H_2 charge/discharge loops.

The typical time evolution of the light transmission signal through the metamembrane for a wavelength of 633 nm

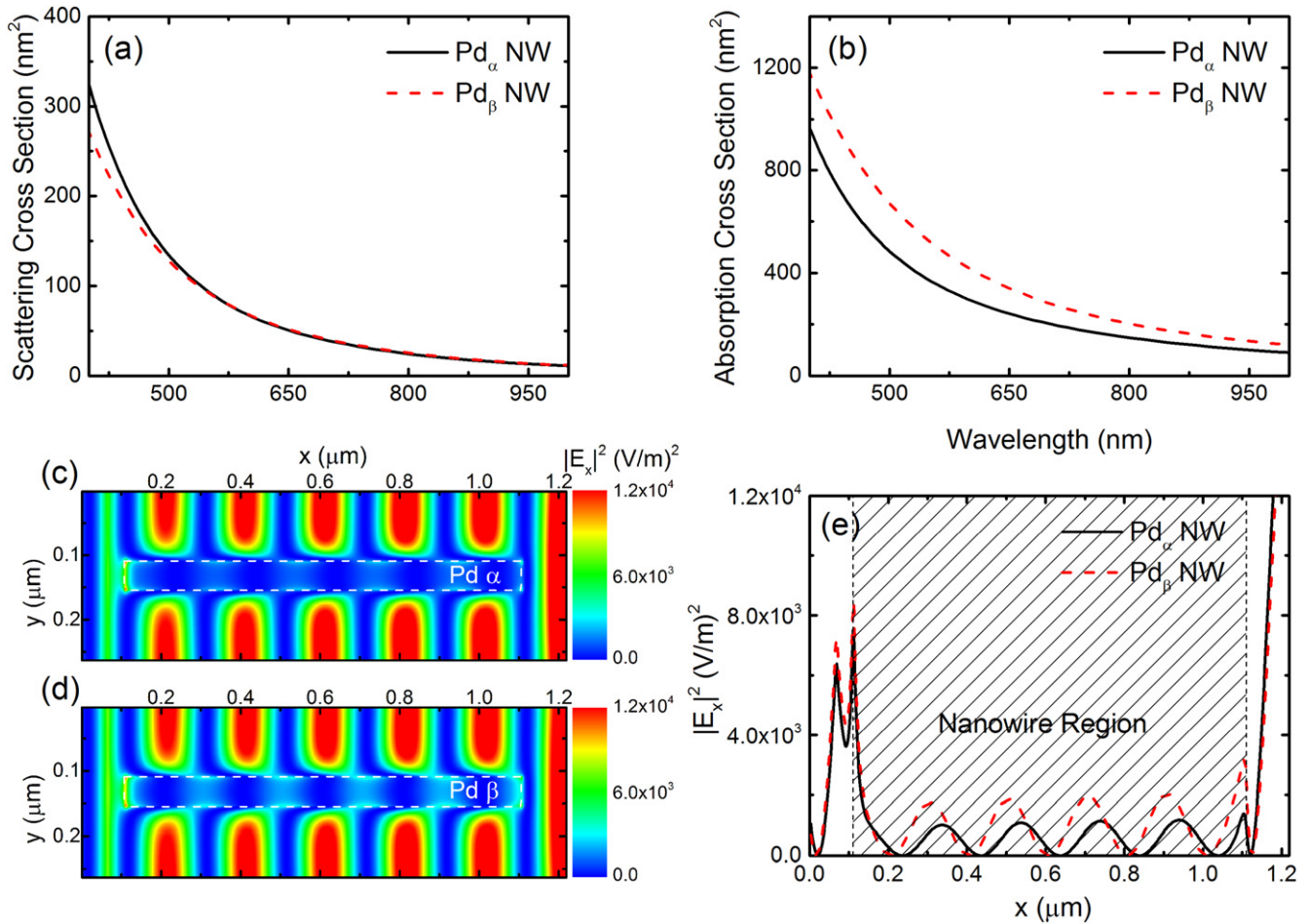


Figure 4. Simulated scattering (a) and absorption (b) cross-sections of a single Pd_α (black line) and Pd_β (dashed red line) NW embedded in Al₂O₃ as a function of wavelength. FDTD simulation of $|E_x|^2$ for a single Pd_α (c) and Pd_β (d) NW embedded in Al₂O₃ and excited by a monochromatic source. The central longitudinal slice of the NW is shown. (e) Field intensity profile centered along the NW for the Pd_α (black line) and Pd_β (dashed red line) NW.

under a H₂ partial pressure of 0.048 atm is presented in figures 5(a) and (b). The former shows an isolated charge/discharge process while the latter presents a continuum sequence of 13 measurement loops. The sensor presents good repeatability (figure 5(b)) and no degradation during the H₂ gas exposures, indicating that both the nanometer-size scale of the Pd NWs and the AAO template protect it against fouling and flaking. The observed time evolution is an exponential-like decay during the charge interval, followed by a slower recovery of the transmission signal when the H₂ is removed from the chamber (figure 5(a)). It is important to note that in all loops the selected charge time (30 min) does not reach the stationary regime, which means that the metamaterial has not reached the maximum H absorption for that pressure. We have selected this transient regime for sensor working operation because it has two important advantages compared to the stationary one. First, the sensor's response time is shorter because it is not necessary to wait until metamembrane saturation, and second, the required discharge time to recover the initial system status is also shorter. In this framework, we have performed the H₂ optical metamaterial sensor calibration by repeating the previously mentioned

experiment at different H₂ partial pressures. We have observed that a clear relation exists between the characteristic time constant of the charge process (defined as $\tau_{5\%}$) and the H₂ partial pressure (figure 5(c)). The $\tau_{5\%}$ time constant corresponds to the waiting time needed to obtain a 5% reduction in light transmission signal relative to the initial one because of the H absorption. This definition is completely arbitrary and is used to show the potential sensing capabilities of the metamaterial. The calibration curve indicates that the fabricated sensor can detect H₂ concentrations in ambient atmospheric conditions below the ignition point (4%) in a few minutes. Above a H₂ partial pressure of 0.16 atm the characteristic time saturates, indicating the concentration limit for sensing. The small difference between the characteristic times observed for the two different gas mixtures (1% and 4%) can be accounted for by the difference between the real concentrations of the gas sources and their nominal values.

The physical origin for the variation of $\tau_{5\%}$ with different H₂ partial pressures results from the H₂ transport process from the surrounding gas into the bulk of the Pd NWs. This occurs in three stages: surface dissociation of H₂ molecules into H atoms, surface adsorption of the H atoms, and finally,

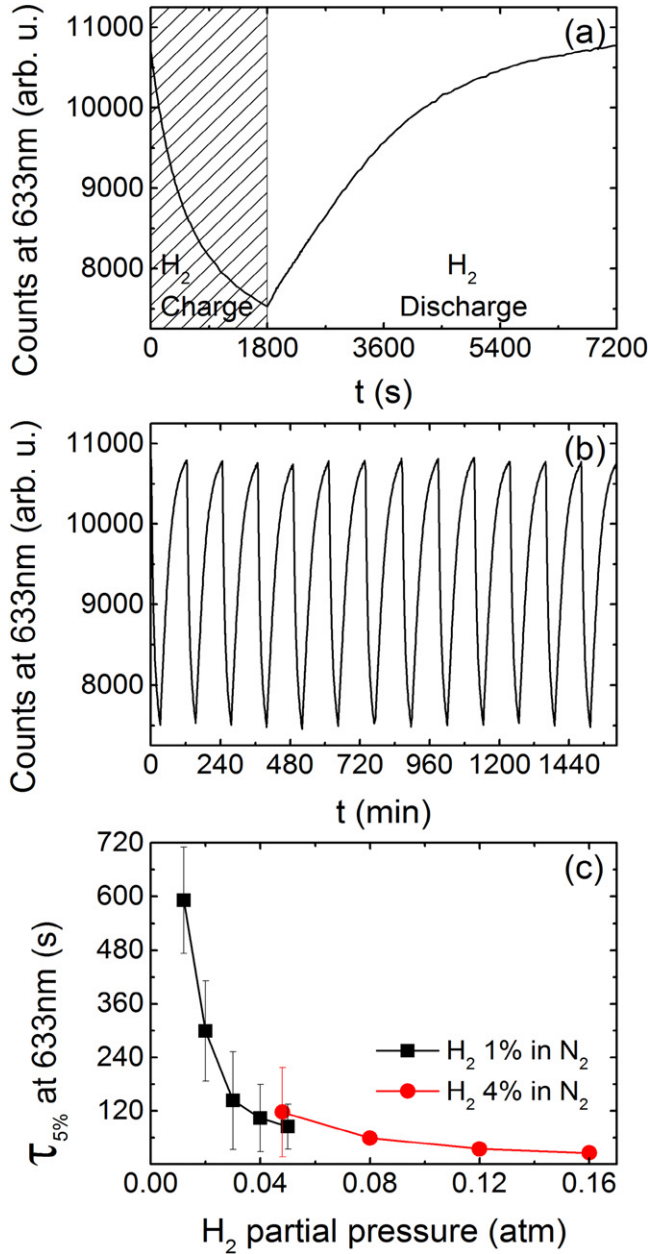


Figure 5. Spectrometer counts at $\lambda = 633$ nm as a function of time for (a) an isolated and (b) a complete sequence of charge/discharge measurements at 0.048 atm of H_2 partial pressure. (c) Characteristic time ($\tau_{5\%}$) measured at $\lambda = 633$ nm as a function of H_2 partial pressure for 1% (black squares) and 4% (red dots) mixtures of H_2 in N_2 .

diffusion of the H atoms inside the Pd [27]. The latter process is very fast, taking about a few μs for typical NW lengths. The value of $\tau_{5\%}$ is therefore limited by H_2 dissociation and H adsorption, which are determined by the number of free dissociation sites in the Pd NW exposed surface. For larger partial pressures, the rate of collisions of the H_2 molecules with the Pd surface increases, leading to a saturation of the dissociation sites. This limits the flow of H into the Pd, and is the reason for the concentration sensing limit.

The sensor's response time and sensitivity are similar to the values reported in [16], where plasmonic enhanced effects

and a much more sophisticated detection setup were used. Comparing with Pd thin film fiberoptic-based sensors, the presented approach is much better in sensitivity, response time and also operation conditions [11]. Note that compared with state-of-the-art resistive sensors, the response time is larger (up to one order of magnitude). However, the presented approach has the advantage of being inherently safe because it is based on optical measurements that avoid the spark risk present in all resistive sensors and works at room temperature.

4.3. Calculation of Pd_β phase concentration

The above results indicate that the fabricated Pd metamaterial works as a variable light absorber depending on the amount of absorbed H atoms. In this framework, the homogenization models previously described can be used not only to predict the metamaterial optical response, but also to estimate the Pd_β phase concentration inside the metamembrane. To achieve this, the equations (3) and (4) were combined, taking into account that the part of the AAO membrane which was not filled with Pd NWs (figure 2(a)) does not affect to the total transmittance of the sample. This is because the corresponding imaginary part of the AAO template refractive index is almost zero, leading to no absorption. In this way, δT as a function of x can be written as follows.

$$\delta T(x) \approx \frac{\exp\left(\frac{-2\pi}{\lambda}[\kappa_{\text{eff}}(x)l_{\text{NW}}]\right) - \exp\left(\frac{-2\pi}{\lambda}[\kappa_{\text{eff}}(0)l_{\text{NW}}]\right)}{\exp\left(\frac{-2\pi}{\lambda}[\kappa_{\text{eff}}(0)l_{\text{NW}}]\right)}, \quad (7)$$

After some straightforward simplifications, the final form for δT is:

$$\delta T(x) \approx \exp\left(\frac{-2\pi}{\lambda}[\kappa_{\text{eff}}(x) - \kappa_{\text{eff}}(0)]l_{\text{NW}}\right) - 1. \quad (8)$$

In equation (8), κ_{eff} represents the Pd metamaterial refractive index's imaginary part, which is, in general, a Pd_β phase concentration function (x). This means that $\kappa_{\text{eff}}(0)$ is the imaginary part of a pure Pd_α metamembrane and $\kappa_{\text{eff}}(1)$ corresponds to a completely hydrogenated one. The values for this function are calculated following the previously mentioned protocol: first, by computing the complex refractive index of the Pd_β/Pd_α mixture inside the NWs by Bruggeman homogenization, and second, by using the Maxwell-Garnett model to obtain the final $\kappa_{\text{eff}}(x)$ for the metamembrane.

In figure 6, the experimental (figure 6(a)) and best fitted (figure 6(b)) δT spectra using the previously explained model are shown for 60 (black line), 300 (red line), 600 (green line) and 1800 (blue line) seconds of H_2 charging time at a partial pressure of 0.048 atm. Equation (8) fits the experimental data well, and allows us to estimate the Pd_β phase concentration inside the metamembrane for each δT measurement. The fitting results indicate that the metamaterial H saturation is not

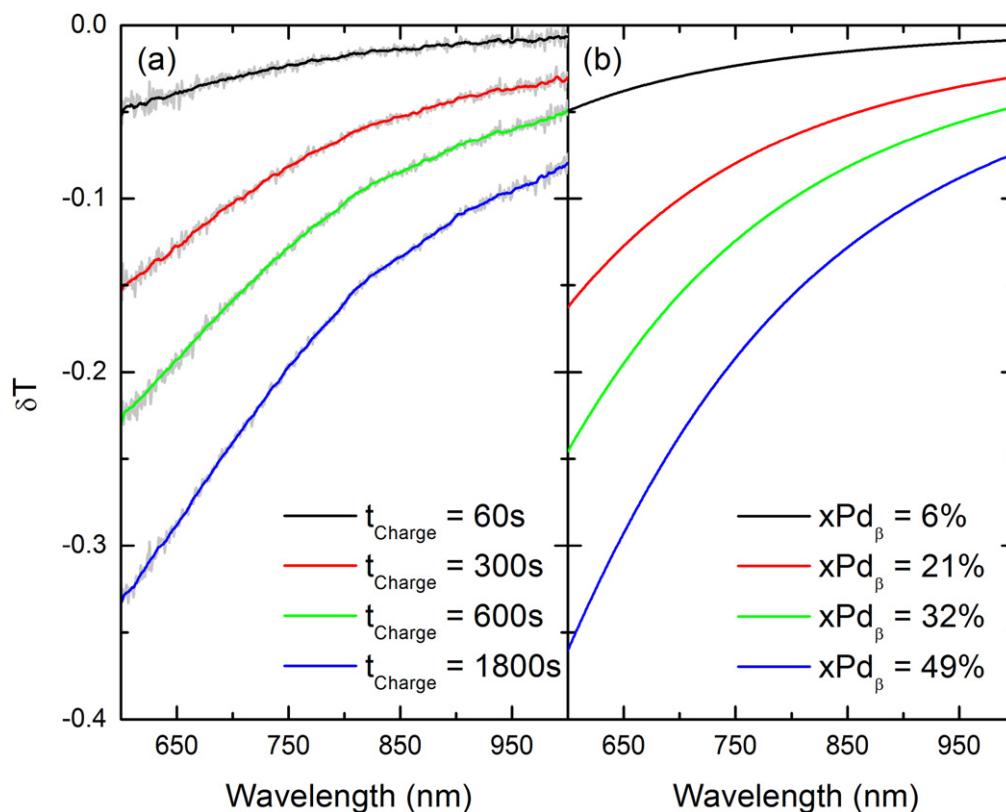


Figure 6. (a) Relative light transmittance change (δT) spectra for different charge instants at 0.048 atm of H_2 partial pressure. (b) Theoretical predictions for δT fitted to the experimental data to obtain the Pd_β phase concentrations ($x\text{Pd}_\beta$).

achieved in agreement with the behavior shown in figure 5. The presented model not only allows us to predict the Pd-based metamaterial H_2 gas sensor behavior, but also opens the door to optically characterize the H diffusion processes inside Pd nanostructures.

5. Conclusions

In summary, we have shown that Pd-AAO metamembranes can be fabricated by using industrially friendly and inexpensive bottom-up techniques, which can be integrated in high-sensitivity and simple H_2 gas optical sensors. The proposed sensor uses the variation in transmitted intensity of non-polarized light through the metamembrane at normal incidence during H_2 exposure. When compared to Pd thin film-based optical sensors, the metamaterial exhibits not only longer durability (due to NW sizes) and increased robustness (due to the AAO membrane exoskeleton), but also anomalous optical absorption, which is the key factor for the sensor's sensitivity. The metamaterial's optical behavior is well described by the proposed homogenization models (the Bruggeman and Maxwell-Garnett theories) showing that the peak broadening, presented by the imaginary part of the metamembrane's effective refractive index after the hydrogenation of Pd NWs, explains the anomalous optical

absorption. This effect has been studied by FDTD simulations revealing that it appears due to the combination of a decrease in the optical impedance between the AAO matrix and the Pd NWs during hydrogenation, and the fact that light is propagating parallel to the NWs. In this way, the light has two different propagation paths, one through the NWs and the other through the AAO matrix. The decrease in the optical impedance between them allows more optical power to be transferred from the AAO to the NWs where it is strongly absorbed. The use of homogenization theories allows prediction of the sensor's optical response and also computation of the Pd_β phase concentration inside the NWs, opening the door to study the H diffusion processes in Pd nanostructures by using optical characterization techniques.

Acknowledgments

The authors acknowledge Prof J M Alameda from the University of Oviedo (Spain) and CINN (CSIC-University of Oviedo-Principado de Asturias, Spain), and J L Menéndez from CINN (CSIC-University of Oviedo-Principado de Asturias, Spain) for the spectroscopic ellipsometry measurements. The authors acknowledge financial support from the projects NORTE-07-0124-FEDER-000070-Multifunctional Nanomaterials, NORTE-07-0124-FEDER-000058 and

PTDC/FIS/119027/2010 (FCOMP-01-0124-FEDER-020713). A Hierro-Rodríguez and J M Teixeira acknowledge support from the FCT of Portugal (Grants SFRH/BPD/90471/2012 and SFRH/BPD/72329/2010, respectively) and POPH/FSE programs.

References

- [1] Kim K T, Sim S J and Cho S M 2006 *IEEE Sens. J.* **6** 509–13
- [2] Rumiche F, Wang H H, Hu W S, Indacchea J E and Wang M L 2008 *Sensors Actuators B* **134** 869–77
- [3] Noh J, Kim H, Lee B S, Cho E and Lee H H 2011 *J. Mater. Chem.* **21** 15935–9
- [4] Ando M 2006 *Trends Anal. Chem.* **25** 937–48
- [5] Hübert T, Boon-Brett L, Black G and Banach U 2011 *Sensors Actuators B* **157** 329–52
- [6] Butler M A 1984 *Appl. Phys. Lett.* **45** 1007–9
- [7] Maier R R J, Jones B J S, Barton J S, McCulloch S, Allsop T, Jones J D C and Bennion I 2007 *J. Opt. A* **9** S45–59
- [8] McDonagh C, Burke C S and MacCraith B D 2008 *Chem. Rev.* **108** 400–22
- [9] Zeng X Q, Latimer M L, Xiao Z L, Panuganti S, Welp U, Kwok W K and Xu T 2011 *Nano Lett.* **11** 262–8
- [10] Zeng X Q *et al* 2011 *ACS Nano* **5** 7443–52
- [11] Westerwaal R J *et al* 2013 *Int. J. Hydrogen Energy* **38** 4201–12
- [12] Ngene P, Radeva T, Slaman M, Westerwaal R J, Schreuders H and Dam B 2014 *Adv. Funct. Mater.* **24** 2374–82
- [13] Lewis F A 1967 *The Palladium Hydrogen System* (New York: Academic Press)
- [14] Chadwick B and Gal M 1993 *Appl. Surf. Sci.* **68** 135–8
- [15] Konospsky V N, Basmanov D V, Alieva E V, Dolgy D I, Olshansky E D, Sekatakii S K and Dietler G 2009 *New J. Phys.* **11** 063049
- [16] Nasir M E, Dickson W, Wurtz G A, Wardley W P and Zayats A V 2014 *Adv. Mater.* **26** 3532–7
- [17] Perrotton C, Westerwaal R J, Javahiraly N, Slaman M, Schreuders H, Dam B and Meyrueis P A 2013 *Opt. Express* **21** 382–90
- [18] Tittl A, Mai P, Taubert R, Dregely D, Liu N and Giessen H 2011 *Nano Lett.* **11** 4366–9
- [19] Langhammer C, Larsson E M, Kasemo B and Zori I 2010 *Nano Lett.* **10** 3529–38
- [20] Liu N, Tang M L, Hentschel M, Giessen H and Alivisatos A P 2011 *Nat. Mater.* **10** 631–6
- [21] Shegai T, Johansson P, Langhammer C and Käll M 2012 *Nano Lett.* **12** 2464–9
- [22] Rakić A D, Djurišić A B, Elazar J M and Majewski M L 1998 *Appl. Opt.* **37** 5271
- [23] Isidorsson J, Giebels I A M E, Arwin H and Griessen R 2003 *Phys. Rev. B* **68** 115112
- [24] Bruggeman D A G 1935 *Ann. Phys.* **24** 636–64
- [25] Maxwell Garnett J C 1904 *Phil. Trans. R. Soc. Lond.* **203** 385–420
- [26] Cai W and Shalaev V 2010 *Optical Metamaterials, Fundamentals and Applications* (New York: Springer)
- [27] Heumann T 1992 *Diffusion in Metallen* (Berlin)
- [28] Vargas W E, Rojas I, Azofeifa D E and Clark N 1966 *Thin Solid Films* **496** 189–96
- [29] Avila J I, Matelon R J, Trabol R, Favre M, Lederman D, Volkmann U G and Cabrera A L 2010 *J. Appl. Phys.* **107** 023504
- [30] Oskooi A F, Roundy D, Ibanescu M, Bermel P, Joannopoulos J D and Johnson S G 2010 *Comput. Phys. Commun.* **181** 687
- [31] Born M and Wolf E 1999 *Principles of Optics* (Cambridge University Press)
- [32] Masuda H and Fukuda K 2001 *Science* **268** 1466–8
- [33] Sousa C T, Leitao D C, Proenca M P, Ventura J, Pereira A M and Araujo J P 2014 *Appl. Phys. Rev.* **1** 031102
- [34] Custodio L M, Sousa C T, Ventura J, Teixeira J M, Marques P V S and Araujo J P 2012 *Phys. Rev. B* **85** 165408
- [35] Sauer G, Brehm G, Schneider S, Nielsch K, Wehrspohn R B, Choi J, Hofmeister H and Gösele U 2002 *J. Appl. Phys.* **91** 3243